Systematics of the temperature-dependent interplane resistivity in $Ba(Fe_{1-x}M_x)_2As_2$ (M = Co, Rh, Ni, and Pd)

M. A. Tanatar,[1,*] N. Ni,[1,2] A. Thaler,[1,2] S. L. Bud'ko,[1,2] P. C. Canfield,[1,2] and R. Prozorov[1,2]

[1]*Ames Laboratory US DOE, Ames, Iowa 50011, USA*

[2]*Department of Physics and Astronomy, Iowa State University, Ames, Iowa 50011, USA*

(Received 11 May 2011; published 27 July 2011)

Temperature-dependent interplane resistivity $\rho_c(T)$ was measured systematically as a function of transition-metal substitution in the iron-arsenide superconductors $Ba(Fe_{1-x}M_x)_2As_2$, M = Ni, Pd, Rh. The data are compared with the behavior found in $Ba(Fe_{1-x}Co_x)_2As_2$, revealing resistive signatures of pseudogap. In all compounds we find resistivity crossover at a characteristic pseudogap temperature T^* from nonmetallic to metallic temperature dependence on cooling. Suppression of T^* proceeds very similarly in cases of Ni and Pd doping and much faster than in similar cases of Co and Rh doping. In cases of Co and Rh doping an additional minimum in the temperature-dependent ρ_c emerges for high dopings, when superconductivity is completely suppressed. These features are consistent with the existence of a charge gap covering part of the Fermi surface. The part of the Fermi surface affected by this gap is notably larger for Ni- and Pd-doped compositions than in Co- and Rh-doped compounds.

DOI: 10.1103/PhysRevB.84.014519 PACS number(s): 74.70.Xa, 72.15.−v, 74.62.−c

I. INTRODUCTION

Pseudogap or partial gap in the electronic structure, affecting some regions of the Fermi surface while leaving others unaffected, is one of the key signatures of the underdoped cuprates.[1] It is revealed through anomalous behaviors of the temperature-dependent resistivity, magnetization, NMR Knight shift, and relaxation rate, as well as in spectroscopic data.[1] Pseudogap shows the same k-space distribution as the superconducting gap[2,3] and is universally observed in hole- and electron-doped cuprates in the underdoped regime.

Features consistent with pseudogap are also clearly found in LaFeAs(O,F) based materials (see Ref. 4 for a review). Because the parent compounds of iron pnictides are metals, the pseudogap here is believed to arise from nesting instability.[4]

In $Ba(Fe_{1-x}M_x)_2As_2$ (BaM122 in the following) substitution of the transition metals into Fe position leads to electron doping. NMR studies suggest the existence of a pseudogap in BaCo122 over the broad doping range including full domain of superconductivity, from magnetically ordered parent compound to nonsuperconducting metal. Existence of pseudogap leads to a temperature-dependent Knight shift K, well described by a formula $K = A + B \times \exp(-T_{PG}/T)$, where the first term describes contribution of the metallic portion of the Fermi surface and the second activated term allows determination of the $T_{PG} \equiv \Delta_{PG}/k_B$ as 560 K ± 150 K at optimal doping.[5–7] At temperatures $T < T^* \ll T_{PG}$ this leads to temperature-independent Knight shift and a crossover to metallic temperature dependence in the interplane resistivity.[8] No discernible features are observed in the in-plane resistivity,[9,10] which suggests that the areas of the Fermi surface affected by pseudogap are rather small and belong to the most warped parts of the Fermi surface, contributing mostly to interplane transport.

In this paper we report a systematic study of the evolution of the interplane resistivity with doping by other transition metals inducing superconductivity in BaM122, M = Rh, Ni, Pd. We show that similar anomalies are observed in the temperature-dependent interplane resistivity for all types of substitution, with the characteristic temperature of resistive crossover being suppressed with doping. The rate of T^* suppression with x is, however, notably higher in Ni- and Pd-doped compositions, even with correction for a difference in the number of added electrons. The doping dependence of the pseudogap feature suggests that it represents an independent energy scale in the problem, different from that of structural and magnetic transitions and superconductivity.

II. EXPERIMENT

Single crystals of $BaFe_2As_2$ doped with Ni, Pd, and Rh were grown as described in detail in previous papers.[11–13] Crystals were thick platelets with large faces corresponding to the tetragonal (001) plane. The actual content of transition metals, x, was determined with wavelength dispersive spectroscopy (WDS) electron probe microanalysis and is used in the following.

We used two-probe resistivity measurements, as justified by ultralow contact resistance of Sn-soldered contacts.[14] The details of sample preparation, sample screening, and selection are identical to those used in our studies of c-axis resistivity in Co-doped material.[8,15,16] The absolute values of the interplane resistivity at room temperature for most compositions stays in the range 1–1.5 mΩ cm; with doping it decreases to approximately 0.5 mΩ cm. For several x compositions we were not able to find crystals with resistivity values lower than 2 mΩ cm, despite the facts that (1) the evolution of the temperature-dependent resistivity for these samples followed the general trend, (2) close in x compositions show usual resistivity values. This limits the accuracy of the absolute ρ_c value determination by approximately a factor of 2.

III. RESULTS

In the left panel of Fig. 1 we plot interplane resistivity of $Ba(Fe_{1-x}Rh_x)_2As_2$, using normalized scale $\rho_c/\rho_c(300\ K)$. To avoid overlapping, the curves are offset progressively upward for higher dopings. The data for the parent compound are

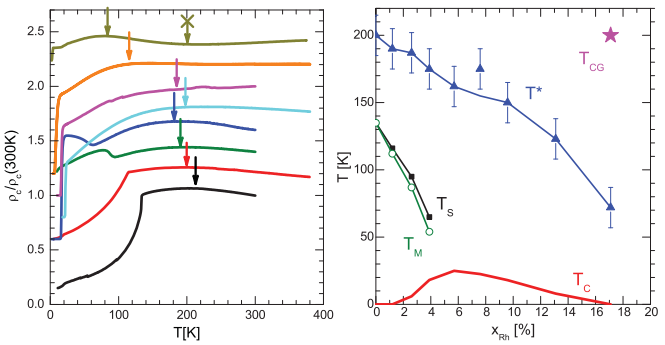

FIG. 1. (Color online) Temperature dependence of the interplane resistivity ρ_c normalized by its value at room temperature $\rho_c(300\ \mathrm{K})$, for samples of $Ba(Fe_{1-x}Rh_x)_2As_2$ with $x \leqslant 0.171$ (slightly above the concentration boundary for the superconducting dome). Lines are offset, from bottom to top, $x_{Rh} = 0$, 0.012, 0.026, 0.039, 0.076, 0.096, 0.131, and 0.171 (left panel). Arrows show a position of the resistivity maximum T^*, crossed arrow shows a position of the resistivity minimum T_{CG}. Right panel shows the $T - x_{Rh}$ phase diagram, in which lines of structural T_S, magnetic T_M, and superconducting T_c states are determined from in-plane resistivity and magnetization measurements; see Ref. 13.

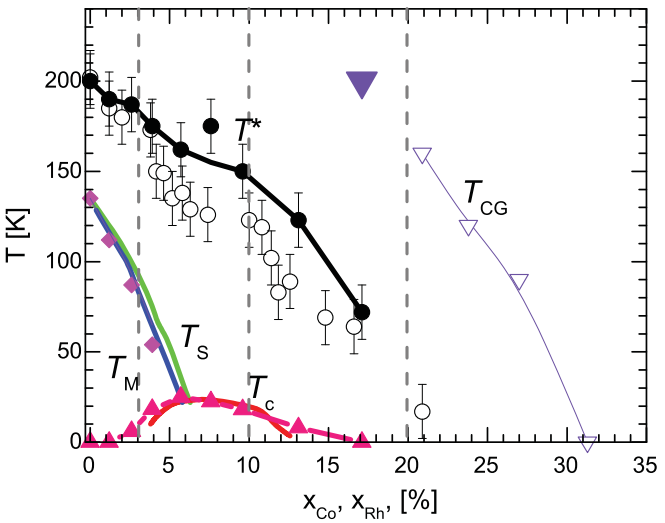

FIG. 2. (Color online) Temperature-concentration phase diagrams of the pseudogap features as revealed from the temperature-dependent interplane resistivity ρ_c in $M = \mathrm{Rh}$ (solid symbols, this study) and $M = \mathrm{Co}$ (open symbols, Ref. 8) doped $Ba(Fe_{1-x}M_x)_2As_2$. Pseudogap features for two types of doping overlap within error bars, similar to the lines of structural T_S, magnetic T_M, and superconducting T_c transitions; Ref. 13. Vertical lines separate composition ranges in which Fermi surface topology changes in $M = \mathrm{Co}$ (Refs. 18– 20).

reproduced from Ref. 16. Several features of the temperature dependence are essentially the same as observed in compositions with Co doping.[8] For low doping $x_{Rh} = 0.012$, $\rho_c(T)$ shows resistivity increase on cooling for $T > T^*$ (marked with an arrow), which is the pseudogap feature in all compositions studied. On reaching a temperature of structural/magnetic transition T_S, resistivity goes down, and decreases monotonically all the way to base temperature, showing some signatures of filamentary superconductivity at about 20 K due to strain.[17] This decrease of resistivity below T_S is similarly observed in lightly Co doped composition $x_{Co} = 0.012$.[8] For higher dopings $x_{Rh} = 0.026$ and $x_{Rh} = 0.39$ resistivity shows an increase below T_S and a drop to zero below superconducting T_c, in complete accord with the behavior found in Co-doped compositions. Finally, for compositions in which structural or magnetic transition is completely suppressed, $x >\sim 0.07$, the position of the resistivity maximum shifts down in temperature and for an ultimate doping $x_{Rh} = 0.171$, when superconductivity is completely suppressed, the resistivity shows shallow minimum, at T_{CG}, marked with crossed arrow in the left panel of Fig. 1. As shown below, this is the same charge-gap temperature as reported in our earlier work.[8] The very fact of the appearance of the minimum at high dopings and even the doping value at which it appears are very similar to those found in Co-doped compounds. We summarize our observations in the temperature-doping, T-x, phase diagram in the right panel of Fig. 1.

In Fig. 2 we compare explicitly the phase diagrams of the pseudogap features in c-axis resistivity of Co- and Rh-doped compounds. Within rather big error bars due to crossover character of features, the diagrams are overlapping. This fact is remarkable, since despite electronic equivalence of Co and Rh doping, the c-axis lattice parameters are different in two materials,[13] and thus it would be natural that this difference should affect characteristic energy scales of the electronic overlap in the interplane direction.

In Figs. 3 and 4 we show the doping evolution of the temperature-dependent interplane resistivity in samples doped

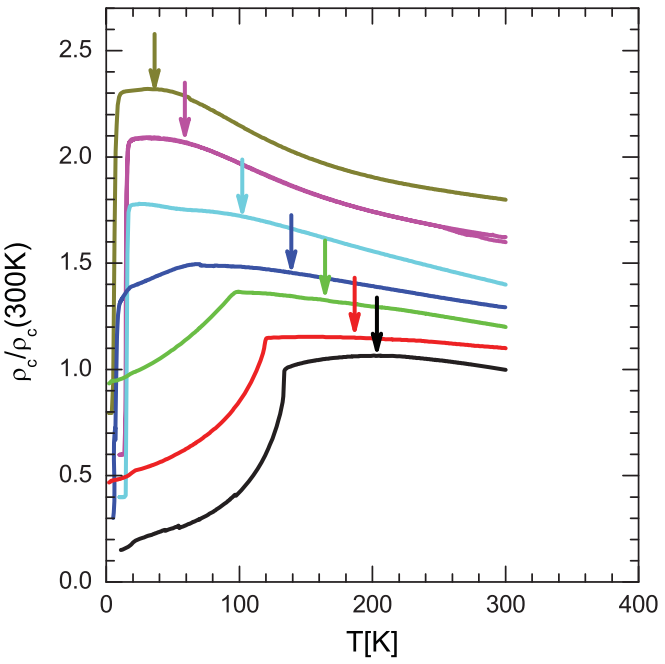

FIG. 3. (Color online) Temperature dependence of the interplane resistivity ρ_c normalized by its value at room temperature $\rho_c(300\ \mathrm{K})$, for samples of $Ba(Fe_{1-x}Ni_x)_2As_2$ with $x \leqslant 0.072$ (slightly above the concentration boundary for the superconducting dome). Lines are offset, from bottom to top, $x_{Ni} = 0$, 0.0067, 0.016, 0.024, 0.032, 0.054, and 0.072. Arrows show a position of the resistivity maximum T^* used to plot the phase diagram; see Fig. 5.

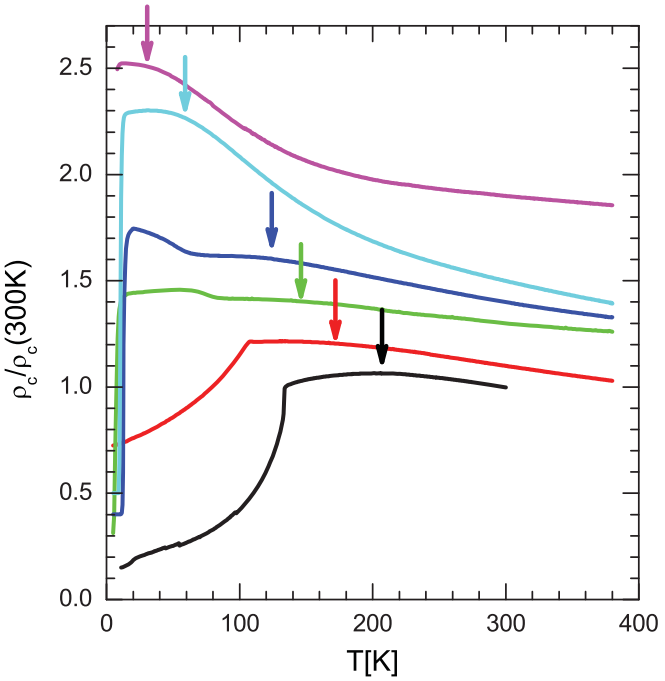

FIG. 4. (Color online) Temperature dependence of the interplane resistivity ρ_c normalized by its value at room temperature $\rho_c(300\ \mathrm{K})$, for samples of $Ba(Fe_{1-x}Pd_x)_2As_2$ with $x \leqslant 0.077$ (slightly above the concentration boundary for the superconducting dome). Lines are offset, from bottom to top, $x_{Pd} = 0, 0.012, 0.021, 0.027, 0.030, 0.053$, and 0.077. Arrows show a position of the resistivity maximum T^* used to plot the phase diagram; see Fig. 5.

with transition metals of group 10 of the Mendeleev periodic table, $3d$ M = Ni and $4d$ M = Pd. These atoms donate two electrons on substituting Fe, and thus the substitution level

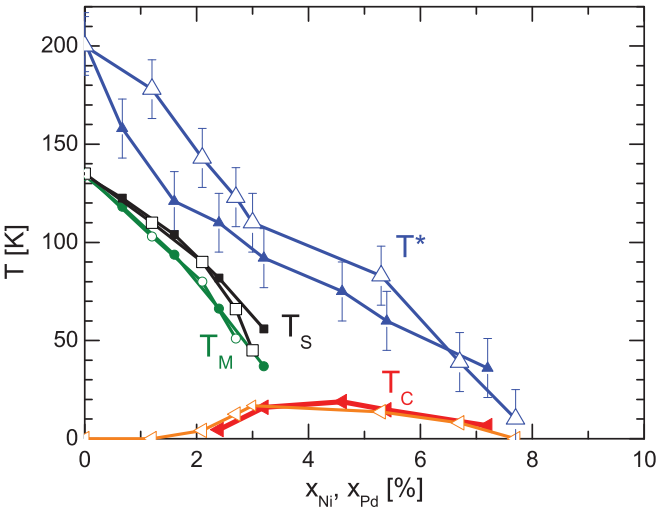

FIG. 5. (Color online) Comparison of the temperature-concentration phase diagrams of the pseudogap features in M = Ni (solid symbols) and M = Pd (open symbols) doped $Ba(Fe_{1-x}M_x)_2As_2$ as determined from interplane resistivity measurements. Lines of structural T_S, magnetic T_M, and superconducting T_c states are determined from in-plane resistivity and magnetization measurements; see Ref. 13. All characteristic features for two types of doping overlap within error bars.

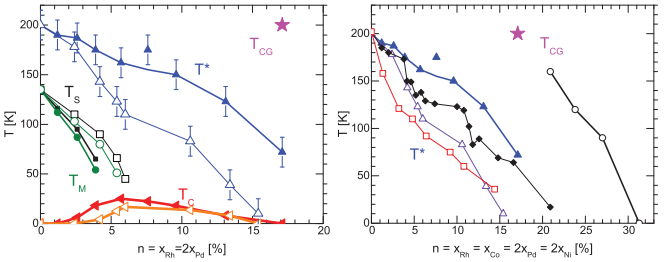

FIG. 6. (Color online) Left panel: comparison of the doping phase diagrams for Rh (solid symbols) and Pd (open symbols) doping, plotted vs concentration of added electrons defined as $n = x_{Rh} = 2x_{Pd}$. Right panel: Phase diagram of the pseudogap features plotted vs $n = x_{Rh} = x_{Co} = 2x_{Pd} = 2x_{Ni}$ for all studied transition metals. Resistivity maximum T^* for Rh (blue solid up triangles), Co (black solid diamonds), Pd (open up triangles), and Ni (red open squares) and resistivity minimum T_{CG} for Rh (solid pink star) and Co (open black circles).

required to induce superconductivity is two times lower than in cases of Co and Rh doping.

Figure 5 shows the doping phase diagrams for Ni and Pd dopings. The suppression of the characteristic temperature of the resistivity maximum T^* is much more rapid for the cases of Ni and Pd doping, and the $T^*(x)$ line in the phase diagram suggests a critical concentration very close to the edge of the superconducting dome. Moreover, for highest doping levels resistivity monotonically decreases with temperature and does not reveal a minimum at T_{CG} as in the cases of Co and Rh doping. On the other hand, similar to the case of Co and Rh (Fig. 2), the phase diagrams of Ni and Pd doping coincide within error bars, see Fig. 5.

IV. DISCUSSION

A. Scaling relations for various dopants

In the systematic study of doping phase diagrams for a variety of transition-metal dopants: Co, Rh, Ni, Pd, Cu, and Cu + Co, it was found that the superconducting transition temperature T_c scales with the number of doped electrons, $n = x_{Co} = x_{Rh} = 2x_{Ni} = 2x_{Pd} = 3x_{Cu}$, while the structural and magnetic transition temperatures scale with the number of dopant atoms $x = x_{Co} = x_{Rh} = x_{Ni} = x_{Pd} = x_{Cu}$. It is therefore interesting if pseudogap features follow either of these scaling relations. While the breakup of $T^*(x)$ scaling is obvious from the comparison of Figs. 2 and 5, in the left panel of Fig. 6 we compare the phase diagrams of Rh- and Pd-doped $BaFe_2As_2$ vs the number of extra electrons n. It is clear that the pseudogap temperature does not scale with n, contrary to the superconducting transition temperature. Because of relatively big error bar in determination of the pseudogap features, in the right panel of Fig. 6 we compare pseudogap features for all four compounds studied. The difference in behavior caused by the dopants from columns 9 (solid symbols) and 10 (open symbols) of the Periodic Table is still clearly resolved, supporting the lack of the scaling of the pseudogap features with n. This difference in the doping dependence implies that

the pseudogap is an independent characteristic energy scale in the phase diagram of Ba122 materials.

B. Relation to Fermi-surface topology

The evolution of the Fermi surface topology in BaCo122 with doping was studied using angle-resolved photoemission spectroscopy and thermopower measurements.[18–20] A sequence of three Lifshits transitions was found, with concentration boundaries at $x_1 = 0.3$, $x_{2\Gamma} = 0.11$, and $x_{2Z} = 0.195$.[18–20] These are shown with gray dash lines in Fig. 2. Unexpectedly, doping evolution of the pseudogap temperature T^* shows little correlation with characteristic features in the Fermi-surface evolution. In particular, the hole pocket near the Γ point in the Brillouin zone changes shape from cylindrical to ellipsoidal at $x_{2\Gamma}$, but merely any feature can be noticed in $T^*(x)$; see Fig. 2. Considering the low anisotropy of electrical resistivity of the compounds, it is not clear which cylinder of the Fermi surface is responsible for carrier activation, however, pseudogap affects most strongly the most warped portions.

Comparison of the temperature-dependent interplane resistivities for heavily overdoped Rh $x_{\mathrm{Rh}} = 0.171$ and Pd $x_{\mathrm{Pd}} = 0.077$ shows an interesting difference. The resistivity monotonically decreases with heating for $x_{\mathrm{Pd}} = 0.077$, top curve in Fig. 4, decreasing from low temperatures to room temperature by a factor of 2. A very similar magnitude of decrease is observed in the sample with $x_{\mathrm{Ni}} = 0.072$, top curve Fig. 3. The magnitude of decrease in $x_{\mathrm{Rh}} = 0.171$, top curve in Fig. 1, is merely 10%, and the curve shows a metallic resistivity increase on heating above ~200 K. This difference suggests that the intact metallic part of the Fermi surface, contributing to the interplane transport, is notably smaller for Ni and Pd doping than in cases of Co and Rh doping. It is interesting if this difference can be found in NMR studies as well.

V. CONCLUSION

In conclusion, our systematic study puts constraints on the possible origin of the anomalous resistivity behavior in transition-metal doped $BaFe_2As_2$. Characteristic temperatures of the pseudogap do not follow the interplane distance, in the samples of the same column of Mendeleev table, as would be naturally expected for variation of the interplane transfer integrals. They neither follow the electron count as would be expected if they were in relation with the Fermi-surface volume or topology (in contrast with the superconducting T_c which scales with n) nor doping evolution of the structural or magnetic transitions. This pushes us to recognize pseudogap as yet another energy scale in the fascinating complexity of the iron pnictide superconductors. Its origin remains as obscure at the moment as the origin of the mysterious pseudogap phase in the cuprates.

ACKNOWLEDGMENTS

We thank A. Kreyssig for useful discussions. Work at the Ames Laboratory was supported by the Department of Energy Basic Energy Sciences under Contract No. DE-AC02-07CH11358. S.L.B. was supported in part by the State of Iowa through the Iowa State University.

*tanatar@ameslab.gov

[1] T. Timusk and B. Statt, Rep. Prog. Phys. **62**, 61 (1999).
[2] F. Ronning, C. Kim, D. L. Feng, D. S. Marshall, A. G. Loeser, L. L. Miller, J. N. Eckstein, I. Bozovic, and Z. X. Shen, Science **282**, 2067 (1998).
[3] T. Kondo, R. Khasanov, T. Takeuchi, J. Schmalian, and A. Kaminski, Nature (London) **457**, 296 (2009).
[4] K. Ishida, Y. Nakai, and H. Hosono, J. Phys. Soc. Jpn. **78**, 062001 (2009).
[5] F. L. Ning, K. Ahilan, T. Imai, A. S. Sefat, R. Jin, M. A. McGuire, B. C. Sales, and D. Mandrus, J. Phys. Soc. Jpn. **77**, 103705 (2008).
[6] F. L. Ning, K. Ahilan, T. Imai, A. S. Sefat, R. Jin, M. A. McGuire, B. C. Sales, and D. Mandrus, J. Phys. Soc. Jpn. **78**, 013711 (2009).
[7] F. L. Ning, K. Ahilan, T. Imai, A. S. Sefat, M. A. McGuire, B. C. Sales, D. Mandrus, P. Cheng, B. Shen, and H.-H Wen, Phys. Rev. Lett. **104**, 037001 (2010).
[8] M. A. Tanatar, N. Ni, A. Thaler, S. L. Bud'ko, P. C. Canfield, and R. Prozorov, Phys. Rev. B **82**, 134528 (2010).
[9] N. Ni, M. E. Tillman, J.-Q. Yan, A. Kracher, S. T. Hannahs, S. L. Bud'ko, and P. C. Canfield, Phys. Rev. B **78**, 214515 (2008).
[10] N. Doiron-Leyraud, P. Auban-Senzier, S. René de Cotret, C. Bourbonnais, D. Jérome, K. Bechgaard, and L. Taillefer, Phys. Rev. B **80**, 214531 (2009).
[11] N. Ni, A. Thaler, J. Q. Yan, A. Kracher, E. Colombier, S. L. Bud'ko, P. C. Canfield, and S. T. Hannahs, Phys. Rev. B **82**, 024519 (2010).
[12] P. C. Canfield, S. L. Bud'ko, N. Ni, J. Q. Yan, and A. Kracher, Phys. Rev. B **80**, 060501(R) (2010).
[13] N. Ni, A. Thaler, A. Kracher, J. Q. Yan, S. L. Bud'ko, and P. C. Canfield, Phys. Rev. B **80**, 024511 (2009).
[14] M. A. Tanatar, N. Ni, S. L. Bud'ko, P. C. Canfield, and R. Prozorov, Supercond. Sci. Technol. **23**, 054002 (2010).
[15] M. A. Tanatar, N. Ni, C. Martin, R. T. Gordon, H. Kim, V. G. Kogan, G. D. Samolyuk, S. L. Bud'ko, P. C. Canfield, and R. Prozorov, Phys. Rev. B **79**, 094507 (2009).
[16] M. A. Tanatar, N. Ni, G. D. Samolyuk, S. L. Bud'ko, P. C. Canfield, and R. Prozorov, Phys. Rev. B **79**, 134528 (2009).
[17] S. R. Saha, N. P. Butch, K. Kirshenbaum, J. Paglione, and P. Y. Zavalij, Phys. Rev. Lett. **103**, 037005 (2009).
[18] Eun Deok Mun, Sergey L. Budko, Ni Ni, Alex N. Thaler, and Paul C. Canfield, Phys. Rev. B **80**, 054517 (2009).
[19] C. Liu, T. Kondo, R. M. Fernandes, A. D. Palczewski, E. D. Mun, N. Ni, A. N. Thaler, A. Bostwick, E. Rotenberg, J. Schmalian, S. L. Bud'ko, P. C. Canfield, and A. Kaminski, Nat. Phys. **6**, 419 (2010).
[20] Chang Liu, A. D. Palczewski, Takeshi Kondo, R. M. Fernandes, E. D. Mun, H. Hodovanets, A. N. Thaler, J. Schmalian, S. L. Bud'ko, P. C. Canfield, and A. Kaminski, e-print arXiv:1011.0980 Phys. Rev. B (in press).